Pages: 125-136 / Vol. 17 / Issue 2 / Summer- Fall 2024

Journal of Aerospace Science and Technology

Journal Homepage: https://jast.ias.ir

Original Research Article

Prediction of Earth Orientation Parameters Using a Hybrid Attention-based CNN-GRU Model with a Coordinate Transformation Approach

Majid Bakhtiari[1]*, Amirhossein Panahyazdan[2], Siavash Sabzy[3]

School of Advanced Technologies, Iran University of Science and Technology, Tehran, Iran

ARARTICLE INFO

Received: 10 February 2024
Revised: 11 March 2024
Accepted: 02 April 2024
Available Online: 02 April 2024

KEYWORDS:

Neural network, Earth Orientation Parameters, Space geodetic techniques, Coordinate transformation, Deep learning

ABSTRACT

The Earth Orientation parameters (EOPs), such as polar motion, universal time, and length of day, play a prominent role in procedures such as monitoring the Earth's rotation, weather modeling, and disaster prevention. This paper estimates the EOPs series based on a combined series approach proposed by the International Earth Rotation and Reference System Observatory between 1962 and 2023, incorporating data from diverse space geodetic techniques, including DORIS, laser ranging (LLR and SLR), GNSS, and VLBI, to create EOPs series. This paper proposes a hybrid deep-learning prediction model, combining a Convolutional Neural Network (CNN) and a Gated Recurrent Unit (GRU) with an attention mechanism. The CNN effectively extracts and enhances features, while the GRU facilitates medium- to long-term predictions based on historical time series data. The attention mechanism prioritizes relevant data aspects, enhancing the model's ability to discern intricate patterns, particularly for Length of Day (LOD) variations, where some covariants affect its pattern and should be considered. One of the most practical applications of these parameters is mapping the points in the terrestrial and celestial reference systems to each other. These predicted EOPs create a high-accuracy coordinate transformation matrix from ECEF to ECI for applications such as high-precision navigation.

DOI:
https://doi.org/10.22034/jast.2024.442700.1174

1 INTRODUCTION

Movements in the fields of navigation, astronomy, and global geodesy demand precise knowledge of the motions of a terrestrial reference frame tied to the Earth and realized by the International Terrestrial Reference Frame (ITRF) with respect to a non-rotating reference system realized by the International Celestial Reference Frame (ICRF). EOPs are the five angles that show the orientation of the Earth in space and allow the transformation between these two reference frames. They relate points in the terrestrial and celestial reference systems[1, 2].

Space geodetic technique uses precise measurements between space objects, such as orbiting satellites and quasars, to determine the positions of points on the Earth, the positions of the Earth's pole, and the Earth's gravity field and geoid [3]. Until today, diverse space-geodetic techniques allow the determination of the EOPs, such as laser ranging to the Moon (LLR), dedicated artificial satellites laser ranging (SLR), very long baseline interferometry (VLBI) from extra-galactic sources, and, more recently, the global positioning system

*Corresponding Author's Email: bakhtiari_m@iust.ac.ir

(GPS) and Doppler Orbitography and Radio positioning Integrated by Satellite (DORIS) systems.

Each of the modern space-geodetic techniques can determine the Earth's orientation parameters. However, each technique has its unique strengths and weaknesses in this regard. Not only is each technique sensitive to a different subset and/ or linear combination of the Earth-orientation parameters, but the averaging time for their determination is different, as is the interval between observations and the precision with which they can be determined. In order to obtain a comprehensive Earth-orientation series, it is necessary to combine the individual series determined by each technique. This combined series is helpful for various scientific studies and data reduction procedures. However, it is essential to consider the differences in the reference frames used by each technique, assign relative weights to each observation, and account for any discrepancies in bias and rate between the Earth-orientation series [4].

There is a rising demand for immediate access to Earth Orientation Parameters in the space navigation and positioning sectors. However, the task of obtaining these parameters in real time is more complex due to the detailed nature of the data processing involved. Consequently, the scientific community is shifting its focus towards the prediction of EOPs to overcome these challenges. Numerous techniques have been developed and applied for EOP prediction, which can be classified into two main groups based on the input data. The first group utilizes information within the EOP time series, such as auto covariance (AC), least squares (LS) collocation, wavelet decomposition, or neural networks. The second group of techniques considers geophysical parameters, such as the axial component of effective angular momentum (EAM) [5].

Considerable investigations have been conducted into determining Earth orientation parameters, each offering unique insights and methodologies. Notably, W. Kosek's research [6] focused on analyzing the efficacy of combining the Least Squares (LS) and Autoregressive (AR) methods, revealing that their integration, referred to as LS+AR, surpasses the individual performance of LS or AR techniques. Moreover, T. Niedzielski [7] explored the fusion of least-squares and multivariate stochastic methods (MAR) to predict UT1–UTC and LOD. This approach leveraged the MAR technique, utilizing atmospheric angular momentum (AAM $\chi 3$) time series as an explanatory variable for LOD or UT1–UTC predictions. In a distinct approach, H. Schuh [8] utilized Artificial Neural Networks (ANN) for EOP prediction, employing the powerful Stuttgart neural network simulator developed at the University of Stuttgart. This endeavor aimed to optimize the neural network topology, learning algorithm, and data input procedure to enhance prediction accuracy. X.Q. Xu [9] adopted a comprehensive strategy, integrating least-squares, autoregressive models, and Kalman filter (LS + AR + Kalman) for short-term prediction of Earth orientation parameters such as length-of-day (LOD), UT1-UTC, and polar motion. Meanwhile, O. Akyilmaz [10] explored Earth orientation parameter estimation utilizing the Adaptive Network-Based Fuzzy Inference System (ANFIS), focusing on LOD and polar motion. Furthermore, Xin Jin [11] applied multi-channel singular spectrum analysis (MSSA) to predict EOPs, particularly polar motion, effectively extracting principal components like trends, annual terms, and Chandler wobbles. Lastly, M. Shahvandi [12] introduced the Neural Differential Learning algorithm for precise time series prediction, employing it specifically for polar motion estimation, contributing to the advancement of EOP prediction techniques.

Earth orientation parameters and prediction comparison campaign have revealed that the integration of the least squares and autocovariance model outperforms other highly accurate proposed models in predicting the EOPs series. This includes techniques such as the Kalman filter, least squares, and autoregressive filtering, least-squares extrapolation and autoregressive prediction, and neural networks. However, it requires being more efficient for medium- and long-term prediction. Nevertheless, the current approaches could be enriched to be more effective, especially in medium- and long-term prediction, and to address the inadequate modeling capabilities of various influencing factors. Although RNNs, including LSTM, have made strides in EOP prediction, the intricate and turbulent characteristics of time series data present a formidable obstacle to achieving accurate predictions. Consequently, this paper aims to propose a hybrid Attention-based CNN–GRU model to predict EOPs [13].

The prior paragraphs mentioned that Earth Orientation Parameters are crucial in applications such as relative navigation and positioning. Therefore, the demand for real-time EOPs is rapidly rising. Although several studies have been conducted in this field, the need for high-precision EOPs still remains. Coordinate transformation, specifically from the fixed frame to the inertial frame, is an essential aspect of navigation that requires EOPs with high accuracy. Thus, in this paper, the predicted EOPs will form a transformation matrix in the mentioned frames.

This paper begins with an overview of the reference systems, namely ECI and ECEF. Subsequently, detailed discussions will be provided on the transformation process between these coordinate systems. Following this, a brief description of the neural network utilized will be outlined, followed by the introduction of the hybrid model. The extraction source of EOPs data will then be introduced. In the results section, the hybrid model will be applied to predict Earth orientation parameters, with the accuracy of the results evaluated using Root Mean Squared Error. Finally, the paper will employ the mentioned model to construct a transformation matrix between the ECI and ECEF frames with high precision. In the last part, the model's error will be scrutinized and discussed.

2 REFERENCE SYSTEMS

To have a comprehensive point of view on coordinate transformation, it is necessary to define the ECI and ECEF frames.

To begin, the Earth Centered Inertial (ECI) coordinate system has its origin at the Earth's center of mass. The Z axis corresponds to the mean north celestial pole of epoch J2000, and the X axis is based on the mean vernal equinox of epoch J2000. The Y axis is the cross product of the Z and X axes in order to be a right-handed system [14].

Earth-Centered-Earth-Fixed (ECEF) is a right-handed Cartesian frame of reference that originated at the center of the Earth. The Z axis is directed along the rotation axis towards the North pole, and the X and Y axes lie in the plane of the equator; the X axis lies in the plane of the Greenwich meridian, and the Y axis completes the right-handed system [14].

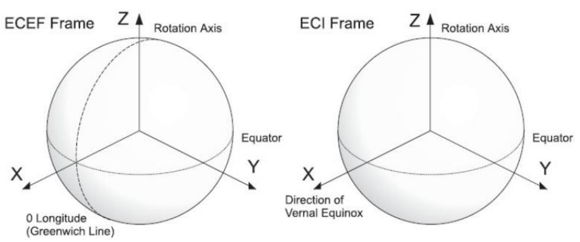

Fig. 1. ECEF and ECI Coordinate System [15].

3 COORDINATE TRANSFORMATION FROM ECEF TO ECI.

The conversion from ECEF to ECI coordinates is a time-varying rotation due primarily to Earth rotation, but it also contains more slowly varying terms for precession, nutation, and polar wander. The ECEF to ECI rotation matrix can be expressed as a composite of four transformations.

$$T_{ECEF\rightarrow ECI} = [M_{pre}{}^{T} M_{nut}{}^{T} M_{rot}{}^{T} M_{pol}{}^{T}] \tag{1}$$

Where M_{pre} , M_{nut}, M_{rot}, and M_{pol} refer to the Transformation matrix associated with the precession between the reference epoch and the epoch t, the Transformation matrix associated with the nutation at epoch t, the Transformation matrix associated with the Earth's rotation around the Conventional Ephemeris Pole (CEP) axis, and the Transformation matrix associated with the polar motion, respectively.

The Long-term alterations in the Earth's average orbit around the Sun impact the ecliptic's orientation, influenced by the gravitational pull of the planets. Consequently, this leads to a corresponding shift in the position of the ecliptic over time, known as precession. The precession matrix consists of three successive rotational matrices.

$$R_P = R_3(-z)R_2(\theta)R_3(-\zeta) = \begin{pmatrix} c_z c_\theta c_\zeta - s_z s_\zeta & -c_z c_\theta s_\zeta - s_z c_\zeta & -c_z s_\theta \\ s_z c_\theta c_\zeta + c_z s_\zeta & -s_z c_\theta s_\zeta + c_z c_\zeta & -s_z s_\theta \\ s_\theta c_\zeta & -s_\theta s_\zeta & c_\theta \end{pmatrix} \tag{2}$$

Where ζ , θ, and z are precession parameters and can be calculated using Eq. (3) to (5).

$$\zeta = 2306''.21881T + 0''.30188T^2 + 0''.017998T^3 \tag{3}$$

$$\theta = 2004''.3109T - 0''.42665T^2 - 0''.041833T^3 \tag{4}$$

$$z = 2306''.21881T + 1''.09468T^2 + 0''.018203T^3 \tag{5}$$

Alongside the gradual precessional movement, the Earth's rotational axis experiences subtle periodic shifts referred to as nutation, as depicted in the Figure. (2). These adjustments arise from both monthly and annual fluctuations in lunar and solar torque. While precession calculations typically account for these variations, nutation represents additional nuances in the Earth's axial orientation.

The principal influencer of nutation is the ever-changing orientation of the lunar orbit concerning the Earth's equator, as denoted by the longitude of the Moon's ascending node, Ω. This phenomenon leads to a recurrent shift of the vernal equinox ($\Delta\psi$), and a change of the obliquity of the ecliptic during the 18.6-year nodal period of the Moon ($\Delta\varepsilon$).

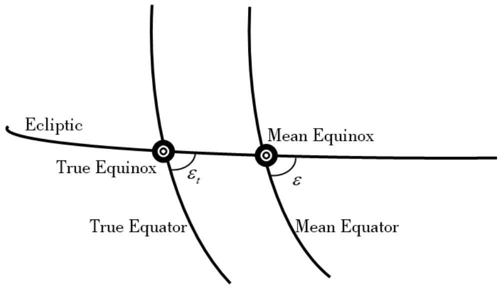

Fig. 2. The shift in the positions of the equator, the ecliptic, and the vernal equinox, caused by nutation.

Finally, the nutation matrix could be described as the product of three successive rotational matrices as mentioned in the Equation. (6).

$$
\begin{aligned}
R_N &= R_1(-\varepsilon-\Delta\varepsilon)R_3(-\Delta\psi)R_1(-\varepsilon) \\
&= \begin{pmatrix} c_{\Delta\psi} & -s_{\Delta\psi}c_\varepsilon & -s_{\Delta\psi}s_\varepsilon \\ s_{\Delta\psi}c_{\varepsilon_t} & c_{\Delta\psi}c_{\varepsilon_t}c_\varepsilon + s_{\varepsilon_t}s_\varepsilon & c_{\Delta\psi}c_{\varepsilon_t}s_\varepsilon + s_{\varepsilon_t}c_\varepsilon \\ s_{\Delta\psi}s_{\varepsilon_t} & c_{\Delta\psi}s_{\varepsilon_t}c_\varepsilon - c_{\varepsilon_t}s_\varepsilon & c_{\Delta\psi}s_{\varepsilon_t}s_\varepsilon - c_{\varepsilon_t}c_\varepsilon \end{pmatrix} \\
&\approx \begin{pmatrix} 1 & -\Delta\psi c_\varepsilon & -\Delta\psi s_\varepsilon \\ \Delta\psi c_{\varepsilon_t} & 1 & -\Delta\varepsilon \\ \Delta\psi s_{\varepsilon_t} & \Delta\varepsilon & 1 \end{pmatrix}
\end{aligned} \tag{6}
$$

Where ε and $\varepsilon_t = \varepsilon + \Delta\varepsilon$ are the mean and true obliquity of the ecliptic at time $T = (JD(TT) - 2451545.0)/36525$. $\Delta\psi$, and $\Delta\varepsilon$ are nutation angles in the longitude and obliquity. As a result of planetary precession, the obliquity of the ecliptic is slightly decreasing, and amounts to Mean obliquity can be calculated through the Equation. (7) [16]

$$
\begin{aligned}
\varepsilon = 84381''.448 &- 46''.8150T \\
&- 0''.00059T^2 \\
&+ 0''.001813T^3
\end{aligned} \tag{7}
$$

The derivation of these values stems from a theory of the secular changes of the Earth's orbital elements. Initially postulated by Newcomb, they were further refined by Lieske [17], building upon prior calculations.

In Equation. (6), the approximation is made by letting $c_{\Delta\psi} = 1$, and $s_{\Delta\psi} = \Delta\psi$ for very small $\Delta\psi$.

The Earth rotation matrix based on the precession-nutation theory is represented as an Equation. (8)

$$R_S = R_3(GAST) \tag{8}$$

Where GAST is Greenwich Apparent Sidereal Time.

The theories of precession and nutation, as established by the International Astronomical Union (IAU), offer valuable insights into the Earth's rotational dynamics. Specifically, they shed light on the precise positioning of the Earth's rotational axis, known as the Celestial Ephemeris Pole (CEP), within the International Celestial Reference System. The rotation around this axis is accurately defined by the Greenwich Mean Sidereal Time (GMST), which measures the angle between the mean vernal equinox and the Greenwich Meridian. Additionally, the Greenwich Apparent Sidereal Time (GAST) measures the hour angle of the true equinox. However, these values differ slightly due to nutation in right ascension, as expressed in equation (9). D. McCarthy's [18] work emphasizes the importance of achieving milliarcsecond accuracy in the equation of the equinoxes, requiring the inclusion of two additional terms. These terms account for a second-order correction resulting from the coupling between precession in longitude and nutation in obliquity within a kinematical definition of apparent sidereal time [16].

$$
\begin{aligned}
GAST = GMST &+ \Delta\psi \cos\varepsilon \\
&+ 0''.00264 \sin\Omega \\
&+ 0''.000063 \sin 2\Omega
\end{aligned} \tag{9}
$$

Where $GMST$ is Greenwich Mean Sidereal Time and can be calculated using the Equation. (10). Ω is the mean longitude of the ascending node of the Moon; the second term on the right-hand side is the nutation of the equinox.

Simon Newcomb [17] implemented a mathematical expression for the fictitious mean Sun, and he defined sidereal time as the hour angle of this fictitious mean Sun. A single expression references Greenwich, providing the Greenwich mean sidereal time at midnight ($GMST_0$) [19]. Expressions for $GMST_0$ at a desired time introduced in Equation. (11).

$$GMST = GMST_0 + \alpha UT1 \tag{10}$$

Archive of SID.ir

$$GMST_0 = 6 \times 3600''.0 + 41 \times 60''.0 + 50''.5481 + 8640184''.812866T_0 + 0''.093104{T_0}^2 - 6''.2 \times 10^{-6}{T_0}^3 \quad (11)$$

$$\alpha = 1.002737909350795 + 5.9006 \times 10^{-11}T_0 - 5.9 \times 10^{-15}{T_0}^2 \quad (12)$$

where $GMST_0$ Greenwich Mean Sidereal Time at midnight on the day of interest. α is the Earth's mean angular rotation in degrees per second and equals to 1 solar day [19]. $UT1$ is the polar motion corrected Universal Time. T_0 is the measuring time in Julian centuries (36,525 days) counted from J2000 to 0h $UT1$ of the measuring day.

Finally, the rotation matrix of polar motion can be represented as:

$$R_M = R_2(-x_p)R_3(-y_p) = \begin{pmatrix} c_{x_p} & s_{x_p}s_{y_p} & s_{x_p} \\ 0 & c_{y_p} & -s_{y_p} \\ -s_{x_p} & c_{x_p} & c_{x_p}c_{y_p} \end{pmatrix} \approx \begin{pmatrix} 1 & 0 & x_p \\ 0 & 1 & -y_p \\ -x_p & y_p & 1 \end{pmatrix} \quad (13)$$

4 HYBRID ATTENTION-BASED CNN-GRU MODEL

As stated in the previous sections, the EOPs are used to implement a model with precision for ECEF to ECI conversion for prospective applications. This study utilizes a hybrid model, the combination of CNN and GRU with an attention mechanism.

5 CNN MODEL

The CNN architecture possesses several building blocks, such as convolution, pooling, and fully connected layers. A regular architecture consists of the reiteration of an accumulation of several convolution layers and a pooling layer, followed by one or more fully connected layers. Forward propagation is the phase where input data is transformed into output through these layers. The CNN network structures can be divided into 1D, 2D, and 3D. It is worth citing that Time series processing is solved mainly by 1D CNN[20].

6 GRU MODEL

A gated Recurrent Unit (GRU) is a robust variant of a standard Recurrent Neural Network (RNN) and, similar to an LSTM, utilizes the combined gating mechanism as a solution to short-term memory. The GRU has an internal mechanism called gates that regulate and even circulate the flow of information. The gates help to learn the GRU cell, whose information is essential to store or erase. Thus, the critical information is passed on to make further predictions. Forget gate and input gates are combined to design an update gate (z_t). The update gate is accountable for preserving the amount of previous memory and new information to be held. (x_t) is a current input vector, and (h_{t-1}) is fundamentally the value computed from the previous adjacent layer. However, (w_z) is a learnable weight matrix for the update gate. Furthermore, the mathematical equations of GRU are represented from Eq. (14) to (17) [21].

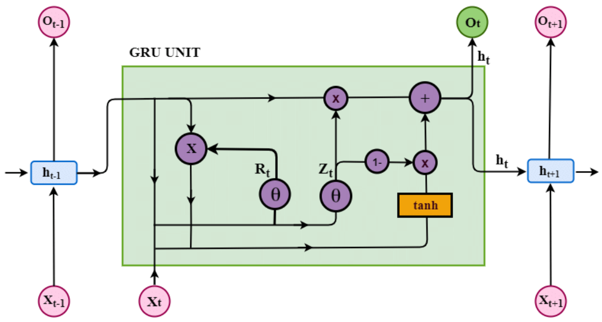

Fig. 3. The Architecture of basic Gated Recurrent Unit (GRU) [21].

$$r_t = \sigma(w_r.[h_{t-1}, x_t]) \quad (14)$$
$$z_t = \sigma(w_z.[h_{t-1}, x_t]) \quad (15)$$
$$\tilde{h}_t = tanh(R_t * [h_{t-1}, x_t]) \quad (16)$$
$$h_t = (1 - z_t) * h_{t-1} + z_t * \tilde{h}_t \quad (17)$$

Where r_t, z_t, $\tilde{h}_t$, and h_t represent reset gate, update gate, candidate hidden state, and final hidden state, respectively.

7 HYBRID MODEL

This paper proposes a deep learning method to predict the EOPs. The proposed method takes advantage of the CNN, the GRU network, and the attention mechanism for boosting performance. The CNN functions well for extracting features from data. The GRU network is perfect for processing temporal data; the attention mechanism allows the GRU network to concentrate on diverse features at different time steps for better prediction accuracy.

In the first place, the documented data and other predictive indicators are taken into the CNN for convolutional processing to extract their essential features. Then, the output results are handed through the GRU network, which can effectively perform long-term time-series prediction, which is an improved version of the LSTM model, and then go through the attention mechanism module to reasonably assign weights and optimize the model, and finally form a CNN-GRU model to predict the historical EOPs[22].

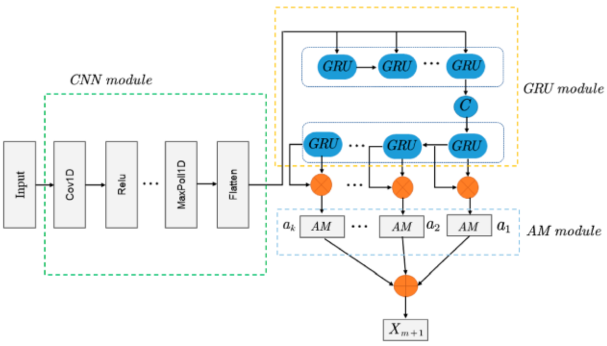

Fig. 4. Attention-Based CNN-GRU Model architecture diagram [22].

8 SOURCES OF EOPS DATA

The International Earth Rotation and Reference System Observatory (IERS) board of directors released the latest version of EOP 14C04 as an IERS reference series, which is available on its website. (accessed on 20 December 2023). Observation data from 1962-01-01 to 2023-01-06 were used in this study for the reasons mentioned in previous sections of this paper. The combined series by IERS was selected for analysis. As can be seen, every method has an apparent limitation in Table (1).

Table 1. Contributions of the different space-geodetic techniques to various products derived by IERS

EOP	VLBI	GNSS	DORIS	Laser Ranging
Polar Motion	✓	✓	✓	✓
LOD	✓	✓	✓	✓
UT1-UTC	✓			
CPO	✓			

9 RESULTS

In this section, the outcome of the model will be introduced, as a consequence of the presence of multiple datasets and diagrams, the selected number of them will be illustrated in this part.

The data used for creating the model are divided into three primary categories, ranging from 1962 to 2023. The first group, spanning from 1962 to 2016, will be utilized to train the model. The second group, from 2016 to 2020, will be used to validate the model. The last group, covering the period from 2020 to 2023, will be employed to test the model.

To gain a better understanding of the x_p, and y_p data, which is the initial group of Earth Orientation Parameters being analyzed, we have presented a portion of the prediction and actual data in Tables (2) and (3). This information will help to make more promising conclusions about the model's accuracy.

Table. 2. Sample of Actual and Predicted x_p from validation Category

DATE	Train Predictions	Actual Data
11/25/2016	0.14571181	0.141313
11/26/2016	0.14375004	0.140256
11/27/2016	0.14205886	0.139
11/28/2016	0.14048404	0.136978
11/29/2016	0.13868807	0.134467

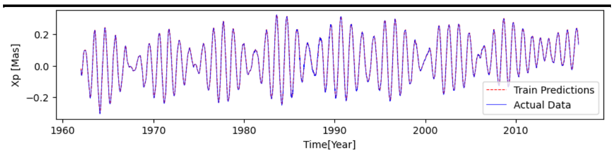

Fig. 5. Variation of Polar motion in x direction for train data.

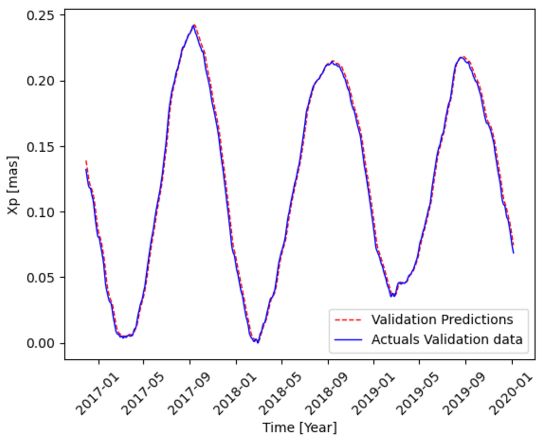

Fig. 6. Variation of Polar motion in x direction for Validation data.

Table. 3. Sample of Actual and Predicted y_p from validation Category

DATE	Train Predictions	Actual Data
11/25/2016	0.26994947	0.268413
11/26/2016	0.26971662	0.268395
11/27/2016	0.26947743	0.268562
11/28/2016	0.26932415	0.268693
11/29/2016	0.269336	0.268366

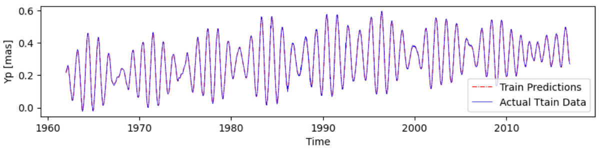

Fig. 7. Variation of Polar motion in y direction for train data.

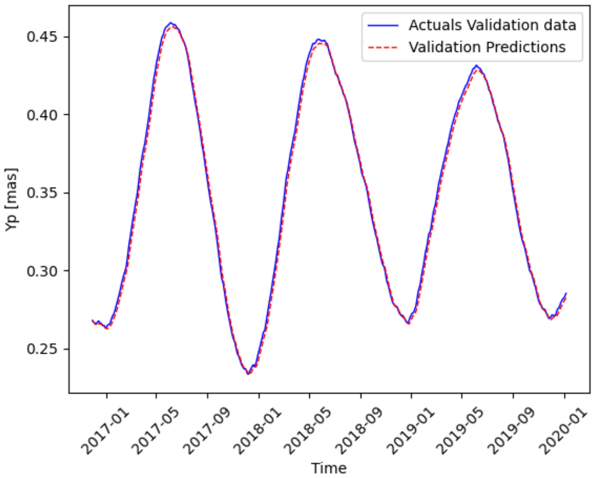

Fig. 8. Variation of Polar motion in y direction for Validation data.

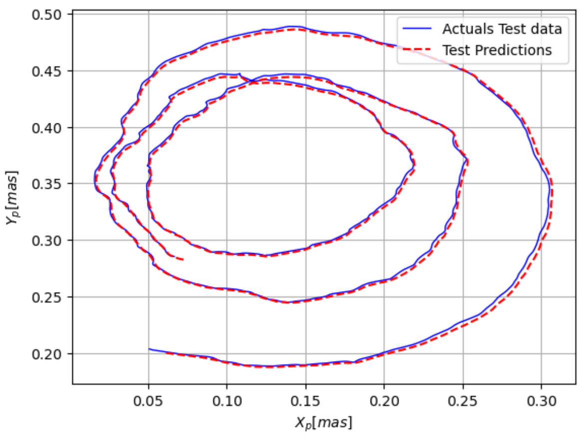

Fig. 9. Illustration of polar motion for test data.

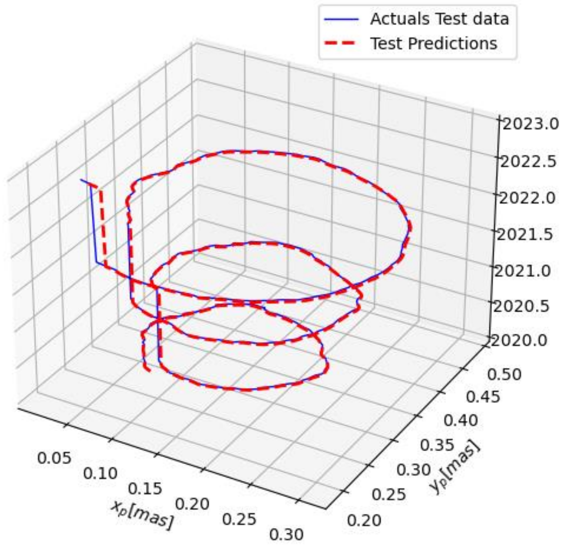

Fig. 10. 3D Illustration of polar motion for test data.

According to Seidelmann's definition [23], polar motion refers to the movement of the Earth's rotational axis with respect to its crust. The polar motion coordinate system is defined by two-dimensional coordinates, where the x-axis points towards the south and aligns with the mean Greenwich meridian, while the y-axis points towards the west. xp and yp are the angles of the pole of date and their variation can be visualized in Figures (5) and (7) for train data and Figures. (6) and (8) for validation data. The training data are employed to instruct the neural network, while the real-world data, in this case, the polar motion (xp and yp), provided by IERS, are juxtaposed with the predicted polar motion generated by the established neural network. Throughout the training phase, it is imperative to evaluate the training process; hence, validation data are utilized to ascertain the efficacy of the network's training. These comparisons are depicted in Figures (5) to (8). Furthermore, the assessment of both training and validation losses indicates the successful training of the network. Consequently, the diagrams representing predicted and validation data exhibit a high degree of similarity. One reason for this accuracy is that the IERS long-term series offers the network more time to train perfectly.

Moreover, as Chen [24] noted, the Earth's pole, the Northern Hemisphere point where the rotation axis intersects the surface, is in constant motion. Dominantly, the movement is circular, which is possible to observe in the plotted diagram using extracted EOPs in the Figure. (9) and (10), following a prograde path with a diameter of several meters [19]. These figures illustrate the periodic oscillation predicted by the neural network for the movement of the Celestial Ephemeris Pole (CEP) around the IERS Reference Pole (IRP), juxtaposed with the authentic periodic oscillation observed in the real-world data.

Analyzing the variation of LOD is an intriguing area of exploration that is supposed to have a close connection with the physics underlying the deep Earth's interior and the motion of Earth's core. Therefore, examining the periodic harmonic components in ΔLOD on interdecadal scales and their physical origins can significantly enhance our comprehension of Earth's core motions, geomagnetic field intensity, and other related phenomena. Similar to polar motion, the neural network's predicted length of day (LOD) was compared to the real-world LOD, provided by the International Earth Rotation and Reference Systems Service (IERS) for both training and validation datasets to meet the study's objective. The results were graphically represented in Figures (11) and (12). Moreover, Table (4) displays the actual and predicted validation data difference for LOD [25].

Table. 4. Sample of Actual and Predicted LOD from validation Category

DATE	Train Predictions	Actual data
11/25/2016	0.00167143	0.0015743
11/26/2016	0.001695956	0.0015314
11/27/2016	0.001729452	0.0014494
11/28/2016	0.001712424	0.0013428
11/29/2016	0.001657027	0.0012618

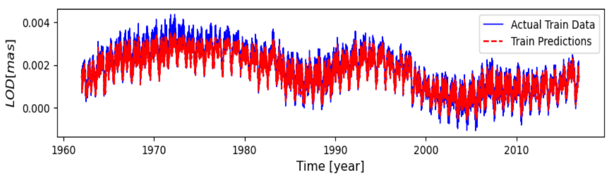

Fig. 11. Variation of LOD for train data.

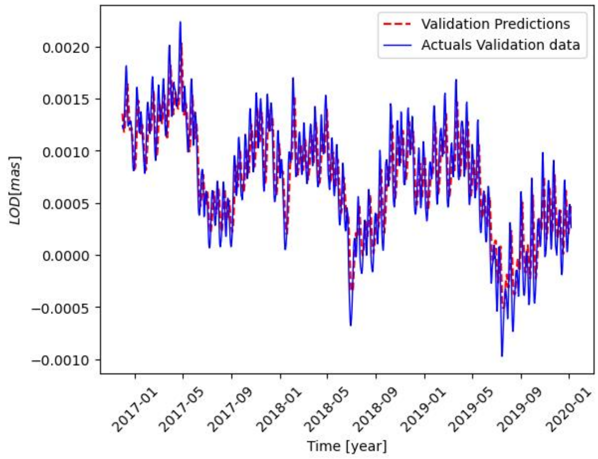

Fig. 12. Variation of LOD for validation data.

To evaluate the precision of EOP prediction, Root Mean Square Error (RMSE) was utilized. It is a statistical measure that describes the average difference between the predicted values and the actual values and can be described as

$$RMSE = \sqrt{\frac{\sum_{1}^{n}(EOP_{Predicted} - EOP_{IERS})^2}{n}} \quad (18)$$

and the outcomes are displayed in the Table. (5).

Table. 5. Root Mean Squared Error of Predicted data

EOP	Data type		
	Train data	Validation data	Test data
X_p	0.01097	0.00747	0.00882
Y_p	0.00569	0.00352	0.00387
LOD	0.00035	0.0003	0.00045
$UT1 - UTC$	0.03617	0.03026	0.00761
dx	0.00021	0.00016	0.0009
dy	0.00014	0.0001	0.00008
$d\varepsilon$	0.00035	0.0003	0.00034
$d\psi$	0.00076	0.00069	0.00071
$TAI - UTC$	0.04763	0.05212	0.0421

In this paper, to assess the model's precision, the EOPs are employed to construct the transformation matrix between ECEF and ECI coordinates in the way mentioned in the prior sections, and investigate it with real-world data. In order to do that, the ESA Soil Moisture and Ocean Salinity (SMOS) satellite's data, which is a low Earth orbit satellite, was employed. It's worth noting that its data was derived from the AGI's database.

An analysis has been carried out to assess the model's performance over a 24-hour period. The findings will be shared; however, only some results will be discussed in detail due to time constraints. Table. (6) displays the real-world data for the velocity and position of SMOS in the ECEF coordinate system on 22 October 2018.

Table. 6. Sample data of the satellite's position and velocity in the ECEF frame on 2018-10-22

Time (Hour)	$\vec{r_x}$ (km)	$\vec{r_y}$ (km)	$\vec{r_z}$ (km)	$\vec{v_x}$ $(\frac{km}{s})$	$\vec{v_y}$ $(\frac{km}{s})$	$\vec{v_z}$ $(\frac{km}{s})$
19	-2732.73	-310.92	-6594.74	-6.66793	2.308991	2.65423
20	5495.605	-2438.23	3844.136	2.925203	-3.20249	-6.19691
21	-5065.76	5023.354	321.4021	1.38088	0.909287	7.383665
21	2279.531	-5136.95	-4410.49	-3.48412	3.405563	-5.77202
23	451.3475	2131.729	6790.799	2.378922	-6.88282	1.998169

Table. 7. Sample data of the Actual Satellite's position and velocity in the ECI frame in 2018-10-22

Time (Hour)	$\vec{r_x}$ (km)	$\vec{r_y}$ (km)	$\vec{r_z}$ (km)	$\vec{v_x}$ $(\frac{km}{s})$	$\vec{v_y}$ $(\frac{km}{s})$	$\vec{v_z}$ $(\frac{km}{s})$
19	-2191.22	1677.89	-6590.78	-6.66793	2.308991	2.65423
20	3628.041	-4799.46	3837.517	2.925203	-3.20249	-6.19691
21	-3699.56	6099.574	328.1861	1.38088	0.909287	7.383665
21	2364.67	-5094.54	-4414.86	-3.48412	3.405563	-5.77202
23	-144.694	2173.17	6791.121	2.378922	-6.88282	1.998169

Table. 8. Sample data of the Transformed Satellite's position and velocity from ECEF to ECI frame in 2018-10-22

Time (Hour)	$\vec{r_x}$ (km)	$\vec{r_y}$ (km)	$\vec{r_z}$ (km)	$\vec{v_x}$ $(\frac{km}{s})$	$\vec{v_y}$ $(\frac{km}{s})$	$\vec{v_z}$ $(\frac{km}{s})$
19	-2191.22	1677.89	-6590.78	-3.30122	6.138404	2.660306
20	3628.041	-4799.46	3837.516	1.341745	-3.95563	-6.19942
21	-3699.56	6099.575	328.1864	1.128294	0.278254	7.381657
21	2364.668	-5094.54	-4414.86	-3.18434	3.514774	-5.76623
23	-144.692	2173.171	6791.121	4.037684	-5.96587	1.990785

Table. 9. The difference between the Actual and predicted position and velocity of SMOS

Differences		
Time (Hour)	$\Delta\vec{r}(km)$	$\overrightarrow{\Delta v}(\frac{km}{s})$
19	0.001136	1.77E-06
20	0.000522	2.29E-06
21	0.001318	2.40E-06
22	0.001831	6.26E-07
23	0.001682	1.13E-06

It is worth remarking that EOPs were also derived from the prediction dataset that was derived in the prior part.

To illustrate the difference between the actual $\vec{r}$, $\vec{v}$ Values and their predicted values in the ECI reference frame in the real world case, we conducted a calculation to determine this difference. The data from this calculation is available for reference in the Table. (8), along with Error diagrams presented in Figure. (13) and (14).

To better evaluate the model's accuracy, we computed the error of the transformation matrix.

The error of positioning and velocity measurement is 0.0003 and 0.004, respectively.

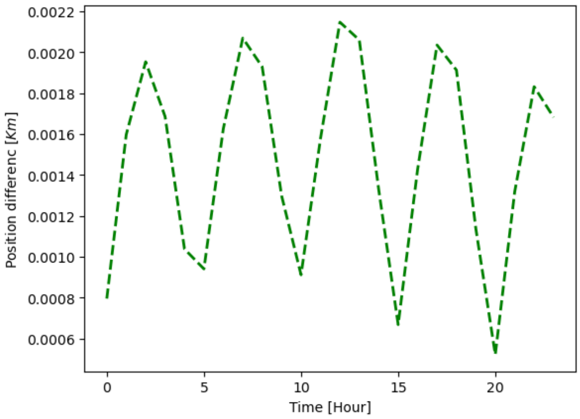

Fig. 13. The diagram of the variation of position in 2018-10-22.

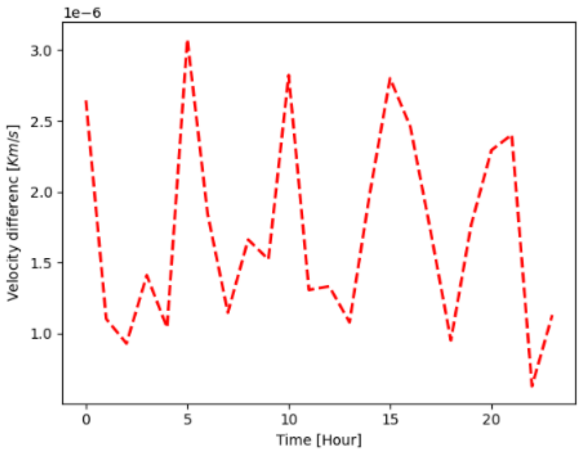

Fig. 14. The diagram of the variation of velocity in 2018-10-22.

10 CONCLUSION

The prediction of Earth orientation parameters is crucial in various fields, such as high-accuracy timing services, precise orbit determination of satellites (POD), and relative navigation. Earlier investigations have highlighted the significance of predicting EOP. This study explored a new deep-learning method to predict EOPs using a recorded dataset from a combined time series presented by IERS for the first time. The study developed an attention-based CNN-GRU model that demonstrated higher accuracy with root mean squared error of approximately 0.0003 and 0.0008 for y_p, and x_p, respectively. This model also demonstrated stability in EOP prediction for the selected period between 1962 and 2023. Besides, a considerable difference in accuracy and stability compared to previous studies in this field can be seen.

Additionally, the study used the predicted EOP dataset to implement the transformation matrix between a fixed and inertial coordinate system. A comparison was then made between the position and velocity of the chosen satellite, SMOS, in the ECI frame with predicted and transformed data. The results revealed the high accuracy of the model. Recently, the precision of monitoring the orientation of the Earth has improved significantly. However, there are still errors that prevent achieving global accuracy due to issues with both celestial and terrestrial reference frames. In order to enhance the precision of the transformation matrix, more accurate EOPs are required. For prospective work, it is necessary to improve the accuracy of neural networks by using novel approaches or using an unexplored architecture for time series prediction. Also, it is possible to assess the accuracy of NN with different applications apart from the coordinate transformation. More research is required to understand the causes of these discrepancies.

CONFLICT OF INTEREST

The authors declare that they have no conflict of interest.

REFERENCES

[1] D. Gambis, "Monitoring Earth orientation using space-geodetic techniques: State-of-the-art and prospective," *J. Geod.*, vol. 78, no. 4, pp. 295–303, 2004, https://doi.org/10.1007/s00190-004-0394-1.

[2] X. Q. Xu, Y. H. Zhou, and C. C. Xu, "Interannual Variation in Earth's Rotation Rate and Its Role as a Climate Change Indicator," *Atmosphere (Basel).*, vol. 14, no. 6, pp. 1–8, 2023, https://doi.org/10.3390/atmos14060982.

[3] S. Modiri et al., "EOP prediction with special focus on SLR," in *Proc. 22nd Int. Workshop on Laser Ranging (IWLR)*, 2010, pp. 1–7.

[4] R. S. Gross, T. M. Eubanks, J. A. Steppe, A.

P. Freedman, J. O. Dickey, and T. F. Runge, "A Kalman-filter-based approach to combining independent Earth-orientation series," J. Geod., vol. 72, pp. 215–235, 1998, https://doi.org/10.1007/s001900050162.

[5] S. Modiri, "On the improvement of earth orientation parameters estimation using modern space geodetic techniques," *M.S. thesis*, Technische Universität Berlin, Germany, 2021.

[6] W. Kosek, M. Kalarus, and T. Niedzielski, "Forecasting of the earth orientation parameters—comparison of different algorithms," in *Proceedings of the Journées Systèmes de Référence Spatiale 2007*, Obs. Paris, pp. 155–158, 2007.

[7] T. Niedzielski and W. Kosek , "Prediction of UT1-UTC, LOD and AAM χ3 by combination of least-squares and multivariate stochastic methods, " *J. Geod.*, vol. 82, pp. 83–92, 2008, https://doi.org/10.1007/s00190-007-0158-9.

[8] H. Schuh, M. Ulrich, D. Egger, J. Müller, and W. Schwegmann, "Prediction of Earth orientation parameters by artificial neural networks, " *J. Geod*., vol. 76, no. 5, pp. 247–258, 2002, https://doi.org/10.1007/s00190-001-0242-5.

[9] X. Q. Xu, Y. H. Zhou, and X. H. Liao, "Short-term Earth orientation parameters predictions by combination of the least-squares, AR model and Kalman filter," *J. Geodyn.*, vol. 62, pp. 83–86, 2012, https://doi.org/10.1016/j.jog.2011.12.001.

[10] O. Akyilmaz and H. Kutterer, "Prediction of Earth rotation parameters by fuzzy inference systems," *J. Geod.*, vol. 78, pp. 82–93, 2004, https://doi.org/10.1007/s00190-004-0374-5.

[11] X. Jin, X. Liu, J. Guo, and Y. Shen, "Analysis and prediction of polar motion using MSSA method," *Earth, Planets Sp.*, vol. 73, 2021, Art. no. 147, https://doi.org/10.1186/s40623-021-01477-2.

[12] M. Kiani Shahvandi, M. Schartner, and B. Soja, , "Neural ODE differential learning and its application in polar motion prediction," *J. Geophys. Res. Solid Earth*, vol. 127, no. 11, 2022, Art. no. e2022JB024775, https://doi.org/10.1029/2022JB024775.

[13] Kalarus, M.; Schuh, H.; Kosek, W.; Akyilmaz, O.; Bizouard, C.; Gambis, D.; Gross, R.; Jovanović, B.; Kumakshev, S.; Kutterer, H. Achievements of the Earth Orientation Parameters Prediction Comparison Campaign. *J. Geod.* **2010**, *84*, 587–596, https://doi.org/10.1007/s00190-010-0387-1.

[14] G. Popescu, "Pixel geolocation algorithm for satellite scanner data," *Scientific Papers. Series E. Land Reclamation, Earth Observation and Surveying, Environmental Engineering*, vol. 3, pp. 127–136, 2014.

[15] G. Lavezzi, Image processing of multiclass satellite tracklets for initial orbit determination based on optical telescopes, *M.S. thesis*, Dept. of Aerospace Science and Technology, Politecnico di Milano, 2018.

[16] Montenbruck, O.; Gill, E.; Lutze, F.H. Satellite Orbits: Models, Methods, and Applications. *Appl. Mech. Rev.* **2002**, *55*, B27–B28, https://doi.org/10.1007/978-3-642-58351-3.

[17] B. D. Lieske, J. H. Lederle, W. Fricke, and B. Morando, "Expressions for the precession quantities based upon the IAU (1976) system of astronomical constants," Astron. Astrophys., vol. 58, no. 1–2, pp. 1–16, 1977.

[18] Dennis D. McCarthy, "IERS Technical note 21," Cent. Bur. MRS - Obs. Paris, no. July, pp. 25–32, 1996.

[19] D. A. Vallado and W. D. McClain, *Fundamentals of Astrodynamics and Applications*, 4th ed., Microcosm Press,p. 1138, 2013.

[20] R. Yamashita, M. Nishio, R. K. G. Do, and K. Togashi, "Convolutional neural networks: An overview and application in radiology," *Insights into Imaging*, vol. 9, pp. 611–629, 2018.

[21] I. Bibi, A. Akhunzada, J. Malik, J. Iqbal, A. Mussaddiq, and S. Kim, "A dynamic DL-driven architecture to combat sophisticated Android malware," *IEEE Access*, vol. 8, pp. 129600–129612, 2020, https://doi.org/10.1109/ACCESS.2020.3009819.

[22] S. Jafari and Y.-C. Byun, "A CNN-GRU Approach to the Accurate Prediction of Batteries' Remaining Useful Life from Charging Profiles," *Computers*, vol. 12, no. 11, 2023, Art. no. 219, https://doi.org/10.3390/computers12110219.

[23] P. K. Seidelmann, "1980 IAU Theory of Nutation: The final report of the IAU Working Group on Nutation," Celest. Mech., vol. 27, no. 1, pp. 79–106, 1982, https://doi.org/10.1007/BF01228952.

[24] S. Adhikari and E. R. Ivins, "Climate-driven polar motion: 2003–2015," *Sci. Adv.*, vol. 2, no. 4, 2016, Art. no. e1501693 https://doi.org/10.1126/sciadv.1501693.

[25] C. C. Hsu, P. S. Duan, X. Q. Xu, Y. H. Zhou, and C. L. Huang, "On the ~ 7 year periodic signal in length of day from a frequency domain stepwise regression method," *J. Geod.*, vol. 95, pp. 1–15, 2021, Art. no. 55, https://doi.org/10.1007/s00190-021-01503-x.

HOW TO SITE THIS ATRICLE

M. Bakhtiari, A. Panahyazdan, S. Sabzy, "Prediction of Earth Orientation Parameters Using a Hybrid Attention-based CNN-GRU Model with a Coordinate Transformation Approach, " *Journal of Aerospace Science and Technology*, Vol. 17, Issue 2, 2024, pp. 125-136.
DOI: https://doi.org/10.22034/jast.2024.442700.1174
URL: https://jast.ias.ir/article_193399.html